Integrated hydrodynamic and machine learning models for compound flooding prediction in a data-scarce estuarine delta

Joko Sampurno[1,2], Valentin Vallaeys[1], Randy Ardianto[3], Emmanuel Hanert[1,4]

[1]Earth and Life Institute (ELI), Université Catholique de Louvain (UCLouvain), Louvain-la-Neuve, 1348, Belgium
[2]Department of Physics, Fakultas MIPA, Universitas Tanjungpura, Pontianak, 78124, Indonesia
[3]Pontianak Maritime Meteorological Station, Pontianak, 78111, Indonesia
[4]Institute of Mechanics, Materials and Civil Engineering (IMMC), Université Catholique de Louvain (UCLouvain), Louvain-la-Neuve, 1348, Belgium

Correspondence to: Joko Sampurno (joko.sampurno@uclouvain.be, jokosampurno@physics.untan.ac.id)

Abstract. Flood forecasting based on hydrodynamic modeling is an essential non-structural measure against compound flooding over the globe. With the risk increasing under climate change, all coastal areas are now in need of flood risk management strategies. Unfortunately, for local water management agencies in developing countries, building such a model is challenging due to the limited computational resources and the scarcity of observational data. We attempt to solve this issue by proposing an integrated hydrodynamic and machine learning approach to predict water level dynamics as a proxy of compound flooding risk in a data-scarce delta. As a case study, this integrated approach is implemented in Pontianak, the densest coastal urban area over the Kapuas River delta, Indonesia. Firstly, we built a hydrodynamic model to simulate several compound flooding scenarios. The outputs are then used to train the machine learning (ML) model. To obtain a robust machine learning model, we consider three machine learning algorithms, i.e., Random Forest, Multi Linear Regression, and Support Vector Machine. Our results show that the integrated scheme works well. The Random Forest (RF) is the most accurate algorithm to model water level dynamics in the study area. Meanwhile, the machine-learning model with the RF algorithm can predict eleven out of seventeen compound flooding events during the implementation phase. It could be concluded that RF is the most appropriate algorithm to build a reliable ML model capable of estimating the river water level dynamics within Pontianak, whose output can be used as a proxy for predicting compound flooding events in the city.

1 Introduction

Compound flooding in low-lying coastal areas is a recognized hazard that can be exacerbated by global warming (Hao and Singh, 2020; Santiago-Collazo et al., 2021; Gori et al., 2022; Hsiao et al., 2021; Ghanbari et al., 2021). Compound flooding hazard is derived from the interaction of storm surge penetration, riverine flooding, and intense rainfall over the areas (as the impact of extreme meteorological events) that coincide or nearly coincide (Bilskie and Hagen, 2018; Ikeuchi et al., 2017; Wahl et al., 2015). This natural hazard can endanger the population and the coastal area's infrastructures, which have been growing fast in the last decade (Bhaskaran et al., 2014). Without appropriate mitigation, the consequences of the hazard can be severe

for the coastal environment (Costabile et al., 2013) and the coastal communities both economically (Karamouz et al., 2014) and socially (Comer et al., 2017).

There are various mechanisms driving compound flooding in low-lying urban coastal areas (Santiago-Collazo et al., 2019). First, the water level increases with the tide, and the sea level rises due to climate change. On top of this, a storm surge may occur. The water can get into the dry land by wave overtopping. Second, extreme precipitation and a high upstream flow discharge can also elevate water in a low-lying delta. In this case, water can overflow and cause flooding as well. These flood pathways are often naturally correlated, so those mechanisms occur coincidentally (or in close succession), creating a compound event and worsening the hazard.

Flood forecasting based on water-level prediction in a tidal river area is an essential non-structural measure against compound flooding (Chan, 2015; Tucci and Villanueva, 1999; Mosavi et al., 2018). Non-structural measures mean any actions to manage the risk of compound flooding without involving a physical construction (UNDRR, 2022), including land-use regulations, flood forecasting, warning systems, floodproofing and disaster prevention, and preparedness and response mechanisms. The water level could be predicted using a process-based or data-based approach. The process-based approach is more commonly used to tackle the water-level prediction issue (Costabile and Macchione, 2015; Ye et al., 2021), but it requires many assumptions to reduce the complexity—making it computationally tractable. The data-based approach, e.g., machine learning and statistical models, can also predict water level changes and compound flooding without the underlying physical attributes and high computational resources (Choi et al., 2020; Wang and Wang, 2020; Assem et al., 2017; Couasnon et al., 2020; Bevacqua et al., 2019). Machine learning involves developing a model that can improve task performance over time by learning from examples, with minimal human efforts instructing them how to do so. Machine learning allows users to test hypotheses and generate confidence bonds for mitigation strategies. Machine learning models can capture and represent a complex input and output relationship using only historical data (Chen and Asch, 2017). For instance, by assuming that flood events are stochastic, machine learning can predict major flood events based on certain probability distributions from the historical discharge data (Mosavi et al., 2018). In some cases, their performance is even more accurate than traditional statistical models (Xu and Li, 2002). In other words, we can prepare strategies to mitigate the flood risks using a machine learning model.

However, building a flood forecasting model in developing countries can be challenging. Implementing a process-based approach requires expensive computational resources (Nayak et al., 2005). Meanwhile, resources owned by local agencies are often limited, so local operational management may not have access to it. Additionally, building a robust machine learning model requires a sufficient amount of data for the training (Naqa et al., 2018), but the availability of observational data in these areas is also limited. Some studies proposed remote sensing techniques (optical and SAR images) as a solution (Mokkenstorm et al., 2021; Kabenge et al., 2017; Haq et al., 2012). Nevertheless, due to the limitation of its time resolution, the technique cannot always detect compound flooding. Therefore, a remote sensing technique is more suitable for detection, monitoring, validation, and mitigation purposes instead of for prediction.

A new paradigm that combines deterministic and machine learning components has been proposed and implemented to tackle data and computational limitations in environmental modeling (Krasnopolsky and Fox-Rabinovitz, 2006; Goldstein and Coco,

2015). However, to the best of our knowledge, no previous modeling frameworks have developed a deterministic model to train a machine learning model for compound flooding studies. As a common practice, compound flood modeling typically uses the coupling of two or more hydrodynamic, hydraulic, or hydrological models (Hsiao et al., 2021; Santiago-Collazo et al., 2021; Ikeuchi et al., 2017). The coupling could be one-way, two-way, or dynamic coupling. Another approach is deep learning and data fusion (Muñoz et al., 2021), and data assimilation (Muñoz et al., 2022).

This study attempts to fill the gap by combining the process-based and data-based approaches as a state-of-the-art framework to predict water level dynamics, a proxy for compound flooding in a data-scarce delta. Firstly, we build a hydrodynamic model to run some flood scenarios in a data-scarce estuary. Then, we create machine learning models trained using the hydrodynamic model's outputs to predict the water level and forecast future floods. To obtain a robust machine learning model, we evaluate three machine learning algorithms and select the most accurate one for our application. As a case study, the integrated framework is implemented in the city of Pontianak, whose population density is the highest within the Kapuas River delta. This city experienced a compound flooding event on 29 December 2018 (Sampurno et al., 2021), and the impact was severe (Madrosid, 2018). At that moment, the water level dynamic is about to go down after passing its peak elevation, when suddenly a strong force pushes it to go up again for a short moment. The interaction between tides, storm surges, and discharges along the tidal river in the Kapuas River delta is responsible for a 30 cm increase in the water level during the event. The finding is expected to assist the local water management agency in assessing their compound flood hazards and mitigating their risk despite the limited data and computational resources.

2 Material and method

2.1 Study area

The Kapuas River is the longest inland river in Indonesia (Goltenboth et al., 2006). The basin is located in the western part of Borneo Island (Fig. 1). The water catchment area spreads over about 93,000 km^2 (about 12.5% of the Borneo Island area, Fig. 1), with about 66.7% of it consisting of forests (Wahyu et al., 2010). The upstream topography comprises hills covered mainly by Acrisol soils (Fig. 2), and the downstream consists of plains with more heterogeneous soil types (Fig. 2), such as *Humic Gleysols* (derived from grass or forest vegetation) and *Dystric Fluvisols* (young soil in alluvial deposits). The river is vital for the local communities as a source of fresh water and a transportation system.

In the last decades, palm oil cultivation and forest fires expanded massively in the Kapuas water catchment (Semedi, 2014; Jadmiko et al., 2017). These circumstances changed the Kapuas hydrological regime and triggered more intense flooding in the river's floodplains. Combined with global sea-level rise, these phenomena could lead to more intense and severe flood events, particularly in the river delta.

The delta of the Kapuas River is still mostly natural, with no dams, dykes, or groins on its downstream. Therefore, the hydrodynamics of the river significantly influences the flood occurrences in the delta. The most populated area over the delta is Pontianak, a city located in the Kapuas Kecil—the middle stream of the second-largest branch of the Kapuas River.

Commented [JS1]: We updated this sentence to:
A new paradigm that combines deterministic and machine learning components has been proposed to tackle data and computational limitations in environmental modeling, such as hybrid climate models (Krasnopolsky and Fox-Rabinovitz, 2006) and an ML model for 2D surface water catchment problems (Maxwell et al., 2021).

As a tidal river, the tidal regime within the Kapuas River delta is mixed but mainly diurnal (Kästner, 2019). The dominant tidal constituent is K1, O1, P1, M2, and S2 (Pauta, 2018). The average tidal amplitude within the delta is set in a microtidal regime, with a mean spring range of 1.45 m at its river mouth (Kästner, 2019).

100   **2.2 Hydrodynamic model description**

To simulate hydrodynamics within the Kapuas River delta, we use the multi-scale hydrodynamic model SLIM 2D (Lambrechts et al., 2008; Gourgue et al., 2009; Remacle and Lambrechts, 2016). The model can simulate hydrodynamic processes along the land-sea continuum, from the river to the ocean (Vallaeys et al., 2018, 2021; Frys et al., 2020; Le et al., 2020b). We simulate compound flooding events based on the water level dynamics for different forcing scenarios using the
105   model. The model solves the 2D Shallow Water Equations (SWE):

$$\frac{\partial H}{\partial t} + \nabla \cdot U = R, \tag{1}$$

$$\frac{\partial U}{\partial t} + \nabla \cdot \left(\frac{UU}{H}\right) + f\boldsymbol{e_z} \times U = \nabla \cdot (\nu \nabla U) + \alpha g H \nabla(H - h) - \frac{Cd}{H^2}|U|U + \frac{1}{\rho}\tau_{wind} - \frac{H}{\rho}\nabla P_{atm} \tag{2}$$

where H is the water column height, ∇ is the horizontal gradient operator, $U = H\overline{\mathbf{u}}$ is the horizontal transport, R is the rainfall, t is the time, $\overline{\mathbf{u}} = (u, v)$ is the depth-averaged horizontal velocity, f is the Coriolis parameter, $\boldsymbol{e_z}$ is the vertical unit vector
110   pointing upward, ν is the horizontal eddy viscosity, α is a constant to define a dry elements ($\alpha = 0$) and wet elements ($\alpha = 1$) (Le et al., 2020a), h is the bathymetry, $g = 9.81$ m/s^2 is the gravitational acceleration, Cd is the bulk drag coefficient, τ_{wind} is the wind stress and ∇P_{atm} is the atmospheric pressure gradient.

2.3 Hydrodynamic model setup and calibration

In order to run the hydrodynamic model, we defined a computational domain that covers both the river and the ocean parts.
115   Next, we generated an unstructured mesh to cover the domain, with a resolution of 50 m over the riverbanks, 400 m over the coast near the river mouth, 1 km over the rest of the coastline, and 5 km over the offshore (Fig. 3). The multi-scale mesh was generated using an algorithm developed by Remacle and Lambrechts (2018). Next, we set the bathymetry constructed from two data sets: first, the river and estuary bathymetry maps, obtained from the Indonesian Navy (Kästner, 2019), and second, the Karimata Strait bathymetry, obtained from BATNAS (BATimetri NASional, 2021). Furthermore, we set the bulk bottom
120   drag coefficients, which are 2.5×10^{-3} over the ocean (which corresponds to a sandy seabed) and 1.9×10^{-2} over the river bed (Kästner et al., 2018). Lastly, we imposed the rainfall, as observed by the Pontianak Maritime Meteorological Station (PMMS).

The hydrodynamic model simulation is forced by wind and atmospheric pressure from ECMWF (Hersbach et al., 2020), and tides from TPXO (Egbert and Erofeeva, 2002). As upstream boundary conditions, we imposed discharge from the Kapuas
125   River and the Landak River. The discharge data were retrieved from the Global Flood Monitoring System (GFMS) (Wu et al., 2014).

We also imposed runoff, which was obtained by converting rainfall over the Kapuas Kecil River catchment area as an inlet water flux at some channels entering the domain. The runoff of every channel was calculated from rainfall data using SWAT+ (Bieger et al., 2017), which considered the pressure, the humidity, and other weather parameter input. Unfortunately, during

130 the tuning of the SWAT model, the correlation between the output of the model (runoff) and the observation data is still low (0.32). However, we decided to use the output as the channels' inlet boundary condition in the hydrodynamic model because the channel runoff volume is much less than the river discharge. Therefore, we assumed that it does not significantly affect the hydrodynamics of the river.

To evaluate the SLIM model performance, we ran a simulation for January 2019 and compared the simulated water elevation

135 with the observations in Pontianak. The model errors correspond to an NSE of 0.87 and an RMSE of 0.12 m (Fig. 4). This RMSE is deemed sufficiently small to consider model outputs as a good proxy of the real system (Moriasi et al., 2015).

We simulated the hydrodynamics with different oceanic, atmospheric, and river forcings to forecast flood events based on the water levels in Pontianak. Based on the Pontianak Maritime Meteorological Station report, the city is flooded when the water level exceeds 2.5 m. We, therefore, set this value as the threshold of a flood event. We ran the hydrodynamic model for ten

140 months and extracted the output hourly to produce the scenarios (see Table 1). Then, we selected 6,000 sample points of the predicted water levels at Pontianak with their associated input dataset. We merged the data as a single dataset to train the machine learning model, encompassing all possible flood events resulting from the combination of the external forcings. The dataset shows that several flooding occurred within the simulations, indicated by sample points with water elevations greater than 2.5 m (Fig. 5).

145 **2.4 Machine learning model**

2.4.1 Dependent and predictor variables

To develop the machine learning models, we used the river water level at Pontianak as the dependent variable. Then, we considered atmospheric, oceanic, and riverine variables as predictors of the water level in the city. Atmospheric variables include average and maximum wind speed, wind direction, precipitation, and average atmospheric pressure. Oceanic variables

150 cover tides at the river mouth, and the riverine variables consist of the Kapuas River, and the Landak River discharges. To evaluate the impact of each predictor before the flood event, we imposed the prior state (one and two hours before) of these parameters (see Table 2). The datasets were recorded hourly and combined with the SLIM output (used in the training and testing phases) and the observational data (used in the implementation phase).

Mutual Information (MI), a statistic tool that can measure the degree of relatedness between variables in a dataset, was

155 implemented to evaluate the relation between each predictor and the dependent variable (Fig. 6). The greater the MI value between two variables, the stronger the relatedness, regardless of how nonlinear its dependency is (Kinney and Atwal, 2014). MI between two variables (X and Y) is obtained from Choi et al. (2020):

$$MI = \sum_{x \in X} \sum_{y \in Y} p(x,y) \, log \left(\frac{p(x,y)}{p(x)-p(y)} \right) \tag{3}$$

160 where $p(x,y)$ is the joint probability distribution.

All predictors considered in the machine learning model have an *MI* coefficient greater than zero, which means all predictor variables impact the river water level in Pontianak (Fig. 6). The relationship between these predictors and the water level could be linear or non-linear (as shown by the MI capturing both relation types). Here, we found that the tidal elevations in the river mouth (X1, X2, and X3) have the most decisive impact on the river water level in the city ($MI > 0.5$), while tidal elevation is

165 observed one hour before (X2) is the strongest one. Next, the wind speed (max and average), the discharges (from both the Kapuas and the Landak river), and the pressure have a moderate relatedness. In contrast, the wind direction and the rainfall have only a weak relatedness ($MI < 0.1$). This means that both parameters have no significant impact.

2.4.2 Machine learning algorithm

Here, we consider three different machine learning algorithms, i.e., random forest (RF), multiple linear regression (MLR), and

170 support vector machine (SVM). RF is a supervised learning algorithm that operates by constructing many decision trees during the training (Breiman, 2001). The algorithm can be implemented for classification or regression. The model aggregates its multiple decision tree outcomes to generate the ultimate output, which is called the sub-sample outcomes (Han et al., 2012). The technique was enhanced by combining bootstrap in its aggregating processes (Breiman, 2001). Using this strategy, the algorithm became an effective tool for classification and regression. In this study, the RF algorithm was obtained from the R

175 randomForest library (Liaw and Wiener, 2002). To obtain the optimal parameter for the RF, we first tune the algorithm by searching for the optimal value of the number of variables randomly sampled as candidates at each split (mtry). As a result, the optimal number is 16 (Fig. 7).

MLR is a statistical technique that uses several explanatory variables to predict the outcome of a response variable (James et al., 2013). This method fits the linear relationship between input features and the target (observed data) using the least-squared

180 approach. In the least-squared approach, the best relationship model will be obtained by minimizing the sum of the squared distance between the calculated values (as model outputs) and the target values (James et al., 2013). This algorithm is the most straightforward approach in machine learning models and is generally used as the baseline method. The MLR algorithm implemented in this study was obtained from the R RWeka library (Hornik et al., 2008).

To obtain the best performance of the MLR algorithm, we did a statistical analysis to evaluate the multicollinearity among the

185 predictor variables using the Variance Inflation Ratio (VIF). Since multicollinearity negatively affects the performance of the MLR model, VIF can help reduce the number of predictors (Alipour et al., 2020). Here, we found that some variables have VIF more significant than 5, which indicates a potentially severe correlation between these variables in the model (Fig. 8). Therefore, combined with the output of *MI* analysis, we removed some variables which have low *MI* and high VIF.

SVM is a supervised machine learning algorithm based on statistical learning frameworks (Gholami and Fakhari, 2017). This

190 method is robust for modeling a complex non-linear relationship. The kernel function transforms the input features into a high-

dimensional space to tackle the complexity. This transforms the non-linear relationship of input features into linear ones. Finally, linear regression is carried out to obtain the ultimate output. Compared with the other algorithms, SVM needs less computational resources because it can be trained only by a few features (Gholami and Fakhari, 2017). Previously, SVM was only implemented for classification purposes, but it has also been implemented for regression purposes after some enhancement. The SVM algorithm implemented in this study was obtained from the R `MARSSVRhybrid` library (MARSSVRhybrid: MARS SVR Hybrid, 2021).

Since kernel function is critical in SVM, we tuned the SVM algorithm to obtain good results by selecting the most appropriate kernel parameter. We tested four kernels, i.e., linear, polynomial, radial basis, and sigmoid, as the candidates. We found that the radial basis kernel performed the best for the SVM algorithm.

2.4.3. Metrics for machine learning model performance evaluation

We use the Nash–Sutcliffe efficiency (NSE) measure to evaluate the models' performance. NSE is used to assess the performance of the machine learning models in producing the predicted water level. A perfect model corresponds to NSE = 1, while a model that has the same predictive skill as the mean of the observed data represents by NSE = 0. Meanwhile, NSE<0 implies that the mean value of observed data predicts better than the model. The closer the NSE value to 1, the better the predictive skill of the model. The NSE coefficient is calculated as follows:

$$NSE = 1 - \frac{\sum_{t=1}^{T} \{H_m^t - H_0^t\}^2}{\sum_{t=1}^{T} (H_0^t - \overline{H_0})^2} \tag{4}$$

where H_m^t represents the water level model at time t, H_0^t represents the observed water level at the same time, and $\overline{H_0}$ is the mean of the observed water level.

Root Mean Square Errors (RMSE) of peaks between predicted water level and observation during the flood events are also used as an additional performance indicator. RMSE is used to represent the model's ability to predict flood events. The RMSE between the model outputs and the observations is calculated by:

$$RMSE = \sqrt{\frac{\sum_{i=1}^{n}(x_i - y_i)^2}{N}} \tag{5}$$

where x_i is the water level as the model's output at the i-th peaks, and y_i is the observed water level at the same time. N is the number of the total peak data.

3 Results

During the training and testing phases, all NSE coefficients are greater than 0.8 both in the training and testing phases, which means that all algorithms perform very well. The most accurate algorithm is RF, followed by SVM and MLR (Fig. 9). As such,

we know that all the tested machine learning algorithms are promising and need to be evaluated in the implementation phase using observational data.

Therefore, we implemented the machine learning models on the selected observational data, which were obtained during the high discharge season for three months in three years when inundations occurred (Dec 2018, Jan 2020, Jan 2021). Fig. 10 shows each proposed algorithm's predicted water levels compared to the observational data. Subsequently, the accuracy of models to predict flooding events, marked by points in Fig. 10, is evaluated.

Even though all algorithms performed very well during the training and testing phases, the performances differed during the implementation phase (Table 3). However, the RF showed high accuracy in three different implementation phases. From the three different observational datasets, RF's NSE values range from 0.61 to 0.72, which is a good performance.

While the MLR algorithm succeeded in the training and testing phases, it only succeeded in the first and third implementation phases, with NSE of 0.72 and 0.65, respectively. The model was less successful in the second implementation phase, with NSE hitting only 0.35 for this implementation dataset.

Next, the SVM algorithm's performance is similar to the MLR algorithm. It succeeded in the training and testing phases but only succeeded in the first and third implementation phases, with NSE reaching 0.71 and 0.63, respectively. However, it failed in the second implementation dataset, with an NSE of only 0.41, which is slightly better than MLR.

Regarding flood events prediction, the RF algorithm also performed better than the other algorithms. It could predict eleven out of seventeen events (65% accuracy). On the other hand, MLR and SVM could only predict six and ten events (35% and 59% accuracy, respectively). Therefore, we know that the RF is the most accurate machine-learning algorithm to predict floods for our test case.

Unfortunately, these three algorithms also predicted false-positive events, i.e., flood events that never occurred during implementation (Table 3). While the RF predicted four false events, the MLR and the SVM predicted three false events. This false event prediction is the shortcoming of the algorithm, which should be addressed in future studies.

4 Discussion

The two main issues that have been tackled in this study are data scarcity and low computational resources for building flood forecasting models based on the water level dynamics in developing countries (Brocca et al., 2020; Singh et al., 2021). Here, we showed that using an approach that combines hydrodynamic and ML models is promising for obtaining a reliable and robust water level model. We succeeded in building and evaluating ML models trained by the hydrodynamic model output; hence, they did not require extensive observational data in their training phase and did not need high computational costs in their implementation. Therefore, the proposed model is reliable for areas where observational data are scarce and computational resources are limited.

Since the proposed model can accurately forecast water levels, local water management agencies can rely on the model outputs for flood forecasting. Since machine learning does not require high computational resources, limited computational resources

will not hinder the assessment and mitigation of compound flooding hazards. Using the model, agencies can re-assess their compound flood hazards and predict future events. Moreover, once they have more observation data, they can use it to re-adjust the proposed model or build a more robust one (Muñoz et al., 2021).

Next, we found that the RF algorithm is the best ML algorithm to predict water level as a proxy for compound flooding in the
255 area of interest. In general, the performances of all tested ML algorithms for water level prediction are reasonable and acceptable. However, considering the NSE values in all implementation phases, the number of flood events that are accurately predicted, and how close the predicted water level is during the events, it could be concluded that the RF performs better than other algorithms. The superiority of the RF algorithm in predicting water levels has also been shown in previous studies in the Upo Wetland (Choi et al., 2020) and the Poyang Lake (Li et al., 2016). Therefore, we proposed a machine learning model with
260 the RF algorithm as the most appropriate model for the study area.

In addition, we found that the tidal elevation measured one-hour prior at the river mouth is the main parameter controlling the river water level in Pontianak. Even though the city is located 20 km from the river mouth, the tidal dynamics still strongly affect the river water level in the city. This result confirms previous studies, revealing that the tide propagation on the Kapuas River dominantly controls the river water level up to 30 km upstream (Sampurno et al., 2021), and still impacts up to 285 km
265 from the river mouth (Kästner et al., 2019).

However, the integrated model proposed in this study also has some limitations. Firstly, the accuracy of the machine learning model built depends on the accuracy of the hydrodynamic model. The more accurate the hydrodynamic model in predicting observational floods, the better the machine learning model will perform. Therefore, we need to tune the hydrodynamic model as accurately as possible. Next, since the rainfall impact on river water level is minor compared to other parameters, the model
270 could not optimally capture urban flooding due to excessive rainfall. Based on the field observation, the city is shortly inundated if rain falls excessively for a few hours. This inundation could be due to the poor quality of the urban drainage system. Unfortunately, this phenomenon is not directly captured by the water level observation located within the river. The increase in the river water level due to the heavy rain is minor. Furthermore, the model relies on the predicted input parameters such as weather parameters and river discharges to predict the future water level. Consequently, the more biased the predictors,
275 the higher the uncertainty in the water-level prediction.

Overall, our integrated approach can provide a model to predict compound flooding driven by the interaction of tide, wind surge from the oceanward, and high discharge from the river upstream. Regarding the limitation of the chosen indicator's capability to capture flood events, we will look for more data and indicators to enhance the model capability in future studies. Moreover, we will reduce the number of predictors to minimize the model output's uncertainty. We will also evaluate mean
280 sea-level rise due to climate change to broaden the model implementation and create better flood mitigation.

5 Conclusion

This study shows that an integrated approach between the hydrodynamic and the machine learning models successfully

Commented [JS9]: We moved this paragraph to a new subsection (2.6. Model limitations).

overcomes modeling river water-level and predicting compound flooding hazards in a data-scarce environment with limited computational resources. Therefore, the approach is suitable for local water management agencies in developing countries that are faced with these issues. However, the accuracy of the machine learning model depends on the accuracy of the hydrodynamic model. If the hydrodynamic model is inaccurate in predicting real-life floods, the machine learning model's accuracy will also be lower. Besides, it has not yet optimally captured the urban flooding due to excessive rainfall. Considering more indicators representing this kind of flooding is essential to enhance the model's capability in the future. Regarding the implementation in Pontianak, we found that the machine learning model with the RF algorithm has the most accurate output compared to the other algorithms. In addition, the tidal elevation, measured one hour prior, is the main predictor for water level modeling in the study area.

Author contribution

JS, VV, and EH conceptualized the research; JS and RA curated the data; JS, VV, and EH analyzed the data; JS wrote the manuscript draft; JS and EH reviewed and edited the manuscript.

Competing interests

The authors declare that they have no conflict of interest.

Acknowledgment

The PhD fellowship of Joko Sampurno is provided by Indonesia Endowment Fund for Education (LPDP) under Grant No. 201712220212183. Computational resources have been provided by the supercomputing facilities of the Université catholique de Louvain (CISM/UCL) and the Consortium des Équipements de Calcul Intensif en Fédération Wallonie Bruxelles (CÉCI) funded by the Fond de la Recherche Scientifique de Belgique (F.R.S.-FNRS) under convention 2.5020.11 and by the Walloon Region.

References

Alipour, A., Ahmadalipour, A., Abbaszadeh, P., and Moradkhani, H.: Leveraging machine learning for predicting flash flood damage in the Southeast US, Environ. Res. Lett., 15, 024011, https://doi.org/10.1088/1748-9326/AB6EDD, 2020.

Assem, H., Ghariba, S., Makrai, G., Johnston, P., Gill, L., and Pilla, F.: Urban Water Flow and Water Level Prediction Based on Deep Learning, Lect. Notes Comput. Sci. (including Subser. Lect. Notes Artif. Intell. Lect. Notes Bioinformatics), 10536

LNAI, 317–329, https://doi.org/10.1007/978-3-319-71273-4_26, 2017.

310   BATimetri NASional: https://tanahair.indonesia.go.id/demnas/#/batnas, last access: 14 July 2021.

Bevacqua, E., Maraun, D., Vousdoukas, M. I., Voukouvalas, E., Vrac, M., Mentaschi, L., and Widmann, M.: Higher probability of compound flooding from precipitation and storm surge in Europe under anthropogenic climate change, Sci. Adv., 5, https://doi.org/10.1126/SCIADV.AAW5531/SUPPL_FILE/AAW5531_SM.PDF, 2019.

Bhaskaran, P. K., Gayathri, R., Murty, P. L. N., Bonthu, S. R., and Sen, D.: A numerical study of coastal inundation and its
315   validation for Thane cyclone in the Bay of Bengal, Coast. Eng., 83, 108–118, https://doi.org/10.1016/J.COASTALENG.2013.10.005, 2014.

Bieger, K., Arnold, J. G., Rathjens, H., White, M. J., Bosch, D. D., Allen, P. M., Volk, M., and Srinivasan, R.: Introduction to SWAT+, a Completely Restructured Version of the Soil and Water Assessment Tool, J. Am. Water Resour. Assoc., 53, 115–130, https://doi.org/10.1111/1752-1688.12482, 2017.

320   Bilskie, M. V. and Hagen, S. C.: Defining Flood Zone Transitions in Low-Gradient Coastal Regions, Geophys. Res. Lett., 45, 2761–2770, https://doi.org/10.1002/2018GL077524, 2018.

Breiman, L.: Random forests, Mach. Learn., 45, 5–32, https://doi.org/10.1023/A:1010933404324, 2001.

Brocca, L., Massari, C., Pellarin, T., Filippucci, P., Ciabatta, L., Camici, S., Kerr, Y. H., and Fernández-Prieto, D.: River flow prediction in data scarce regions: soil moisture integrated satellite rainfall products outperform rain gauge observations in West
325   Africa, Sci. Reports 2020 101, 10, 1–14, https://doi.org/10.1038/s41598-020-69343-x, 2020.

Buchhorn, M., Lesiv, M., Tsendbazar, N.-E., Herold, M., Bertels, L., and Smets, B.: Copernicus Global Land Cover Layers—Collection 2, Remote Sens. 2020, Vol. 12, Page 1044, 12, 1044, https://doi.org/10.3390/RS12061044, 2020.

Chan, N. W.: Impacts of Disasters and Disaster Risk Management in Malaysia: The Case of Floods, Resil. Recover. Asian Disasters, 239–265, https://doi.org/10.1007/978-4-431-55022-8_12, 2015.

330   Chen, J. H. and Asch, S. M.: Machine Learning and Prediction in Medicine — Beyond the Peak of Inflated Expectations, N. Engl. J. Med., 376, 2507, https://doi.org/10.1056/NEJMP1702071, 2017.

Choi, C., Kim, J., Han, H., Han, D., and Kim, H. S.: Development of Water Level Prediction Models Using Machine Learning in Wetlands: A Case Study of Upo Wetland in South Korea, 12, 93, https://doi.org/10.3390/W12010093, 2020.

Comer, J., Indiana Olbert, A., Nash, S., and Hartnett, M.: Development of high-resolution multi-scale modelling system for
335   simulation of coastal-fluvial urban flooding, Nat. Hazards Earth Syst. Sci., 17, 205–224, https://doi.org/10.5194/NHESS-17-205-2017, 2017.

Costabile, P. and Macchione, F.: Enhancing river model set-up for 2-D dynamic flood modelling, Environ. Model. Softw., 67,

89–107, https://doi.org/10.1016/J.ENVSOFT.2015.01.009, 2015.

Costabile, P., Costanzo, C., and Macchione, F.: A storm event watershed model for surface runoff based on 2D fully dynamic
340   wave equations, Hydrol. Process., 27, 554–569, https://doi.org/10.1002/HYP.9237, 2013.

Couasnon, A., Eilander, D., Muis, S., Veldkamp, T. I. E., Haigh, I. D., Wahl, T., Winsemius, H. C., and Ward, P. J.: Measuring
compound flood potential from river discharge and storm surge extremes at the global scale, Nat. Hazards Earth Syst. Sci., 20,
489–504, https://doi.org/10.5194/NHESS-20-489-2020, 2020.

MARSSVRhybrid: MARS SVR Hybrid: https://cran.r-project.org/web/packages/MARSSVRhybrid/index.html, last access:
345   23 September 2021.

Egbert, G. D. and Erofeeva, S. Y.: Efficient inverse modeling of barotropic ocean tides, J. Atmos. Ocean. Technol., 19, 183–
204, 2002.

Farr, T. G., Rosen, P. A., Caro, E., Crippen, R., Duren, R., Hensley, S., Kobrick, M., Paller, M., Rodriguez, E., Roth, L., Seal,
D., Shaffer, S., Shimada, J., Umland, J., Werner, M., Oskin, M., Burbank, D., and Alsdorf, D. E.: The Shuttle Radar
350   Topography Mission, Rev. Geophys., 45, 2004, https://doi.org/10.1029/2005RG000183, 2007.

Frys, C., Saint-Amand, A., Le Hénaff, M., Figueiredo, J., Kuba, A., Walker, B., Lambrechts, J., Vallaeys, V., Vincent, D., and
Hanert, E.: Fine-Scale Coral Connectivity Pathways in the Florida Reef Tract: Implications for Conservation and Restoration,
Front. Mar. Sci., 7, 312, https://doi.org/10.3389/FMARS.2020.00312/BIBTEX, 2020.

Ghanbari, M., Arabi, M., Kao, S. C., Obeysekera, J., and Sweet, W.: Climate Change and Changes in Compound Coastal-
355   Riverine Flooding Hazard Along the U.S. Coasts, Earth's Futur., 9, e2021EF002055, https://doi.org/10.1029/2021EF002055,
2021.

Gholami, R. and Fakhari, N.: Support Vector Machine: Principles, Parameters, and Applications, in: Handbook of Neural
Computation, Elsevier Inc., 515–535, https://doi.org/10.1016/B978-0-12-811318-9.00027-2, 2017.

Goldstein, E. B. and Coco, G.: Machine learning components in deterministic models: Hybrid synergy in the age of data, Front.
360   Environ. Sci., 3, 33, https://doi.org/10.3389/FENVS.2015.00033/BIBTEX, 2015.

Goltenboth, F., Timotius, K. H., Milan, P. P., and Margraf, J.: Ecology of insular Southeast Asia: the Indonesian archipelago,
Elsevier B.V., 2006.

Gori, A., Lin, N., Xi, D., and Emanuel, K.: Tropical cyclone climatology change greatly exacerbates US extreme rainfall–
surge hazard, Nat. Clim. Chang. 2022 122, 12, 171–178, https://doi.org/10.1038/s41558-021-01272-7, 2022.

365   Gourgue, O., Comblen, R., Lambrechts, J., Kärnä, T., Legat, V., and Deleersnijder, E.: A flux-limiting wetting–drying method
for finite-element shallow-water models, with application to the Scheldt Estuary, Adv. Water Resour., 32, 1726–1739,
https://doi.org/10.1016/J.ADVWATRES.2009.09.005, 2009.

Han, J., Kamber, M., and Pei, J.: Data Mining: Concepts and Techniques, Elsevier Inc., https://doi.org/10.1016/C2009-0-61819-5, 2012.

370 Hao, Z. and Singh, V. P.: Compound Events under Global Warming: A Dependence Perspective, J. Hydrol. Eng., 25, 03120001, https://doi.org/10.1061/(ASCE)HE.1943-5584.0001991, 2020.

Haq, M., Akhtar, M., Muhammad, S., Paras, S., and Rahmatullah, J.: Techniques of Remote Sensing and GIS for flood monitoring and damage assessment: A case study of Sindh province, Pakistan, Egypt. J. Remote Sens. Sp. Sci., 15, 135–141, https://doi.org/10.1016/J.EJRS.2012.07.002, 2012.

375 Hersbach, H., Bell, B., Berrisford, P., Hirahara, S., Horányi, A., Muñoz-Sabater, J., Nicolas, J., Peubey, C., Radu, R., Schepers, D., Simmons, A., Soci, C., Abdalla, S., Abellan, X., Balsamo, G., Bechtold, P., Biavati, G., Bidlot, J., Bonavita, M., Chiara, G., Dahlgren, P., Dee, D., Diamantakis, M., Dragani, R., Flemming, J., Forbes, R., Fuentes, M., Geer, A., Haimberger, L., Healy, S., Hogan, R. J., Hólm, E., Janisková, M., Keeley, S., Laloyaux, P., Lopez, P., Lupu, C., Radnoti, G., Rosnay, P., Rozum, I., Vamborg, F., Villaume, S., and Thépaut, J.: The ERA5 global reanalysis, Q. J. R. Meteorol. Soc., 146, 1999–2049, 380 https://doi.org/10.1002/qj.3803, 2020.

Hornik, K., Buchta, C., and Zeileis, A.: Open-source machine learning: R meets Weka, Comput. Stat., 24, 225–232, https://doi.org/10.1007/S00180-008-0119-7, 2008.

Hsiao, S. C., Chiang, W. S., Jang, J. H., Wu, H. L., Lu, W. S., Chen, W. B., and Wu, Y. T.: Flood risk influenced by the compound effect of storm surge and rainfall under climate change for low-lying coastal areas, Sci. Total Environ., 764, 144439, 385 https://doi.org/10.1016/J.SCITOTENV.2020.144439, 2021.

Ikeuchi, H., Hirabayashi, Y., Yamazaki, D., Muis, S., Ward, P. J., Winsemius, H. C., Verlaan, M., and Kanae, S.: Compound simulation of fluvial floods and storm surges in a global coupled river-coast flood model: Model development and its application to 2007 Cyclone Sidr in Bangladesh, J. Adv. Model. Earth Syst., 9, 1847–1862, https://doi.org/10.1002/2017MS000943, 2017.

390 Jadmiko, S. D., Murdiyarso, D., and Faqih, A.: Climate Changes Projection for Land and Forest Fire Risk Assessment in West Kalimantan, IOP Conf. Ser. Earth Environ. Sci., 58, 012030, https://doi.org/10.1088/1755-1315/58/1/012030, 2017.

James, G., Witten, D., Hastie, T., and Tibshirani, R.: An Introduction to Statistical Learning with Applications in R, 8th ed., Springer, New York, 2013.

Kabenge, M., Elaru, J., Wang, H., and Li, F.: Characterizing flood hazard risk in data-scarce areas, using a remote sensing and 395 GIS-based flood hazard index, Nat. Hazards, 89, 1369–1387, https://doi.org/10.1007/S11069-017-3024-Y, 2017.

Karamouz, M., Zahmatkesh, Z., Goharian, E., and Nazif, S.: Combined Impact of Inland and Coastal Floods: Mapping Knowledge Base for Development of Planning Strategies, J. Water Resour. Plan. Manag., 141, 04014098,

https://doi.org/10.1061/(ASCE)WR.1943-5452.0000497, 2014.

Kästner, K.: Multi-scale monitoring and modelling of the Kapuas River Delta, Wageningen University,
400 https://doi.org/10.18174/468716, 2019.

Kästner, K., Hoitink, A. J. F., Torfs, P. J. J. F., Deleersnijder, E., and Ningsih, N. S.: Propagation of tides along a river with a sloping bed, J. Fluid Mech., 872, 39–73, https://doi.org/10.1017/JFM.2019.331, 2019.

Kinney, J. B. and Atwal, G. S.: Equitability, mutual information, and the maximal information coefficient, Proc. Natl. Acad. Sci. U. S. A., 111, 3354–3359, https://doi.org/10.1073/pnas.1309933111, 2014.

405 Krasnopolsky, V. M. and Fox-Rabinovitz, M. S.: A new synergetic paradigm in environmental numerical modeling: Hybrid models combining deterministic and machine learning components, Ecol. Modell., 191, 5–18, https://doi.org/10.1016/J.ECOLMODEL.2005.08.009, 2006.

Lambrechts, J., Hanert, E., Deleersnijder, E., Bernard, P. E., Legat, V., Remacle, J. F., and Wolanski, E.: A multi-scale model of the hydrodynamics of the whole Great Barrier Reef, Estuar. Coast. Shelf Sci., 79, 143–151,
410 https://doi.org/10.1016/J.ECSS.2008.03.016, 2008.

Le, H.-A., Lambrechts, J., Ortleb, S., Gratiot, N., Deleersnijder, E., and Soares-Frazão, S.: An implicit wetting-drying algorithm for the discontinuous Galerkin method: application to the Tonle Sap, Mekong River Basin, Environ. Fluid Mech., 20, 923–951, https://doi.org/10.1007/s10652-019-09732-7, 2020a.

Le, H. A., Gratiot, N., Santini, W., Ribolzi, O., Tran, D., Meriaux, X., Deleersnijder, E., and Soares-Frazão, S.: Suspended
415 sediment properties in the Lower Mekong River, from fluvial to estuarine environments, Estuar. Coast. Shelf Sci., 233, 106522, https://doi.org/10.1016/J.ECSS.2019.106522, 2020b.

Li, B., Yang, G., Wan, R., Dai, X., and Zhang, Y.: Comparison of random forests and other statistical methods for the prediction of lake water level: a case study of the Poyang Lake in China, Hydrol. Res., 47, 69–83, https://doi.org/10.2166/NH.2016.264, 2016.

420 Liaw, A. and Wiener, M.: Classification and regression by randomForest, R News, 2, 18–22, 2002.

Madrosid: Cerita Warga, Detik-detik Banjir Rob Melanda Kota Pontianak, Trib. Pontianak, 2018.

Mokkenstorm, L. C., van den Homberg, M. J. C., Winsemius, H., and Persson, A.: River Flood Detection Using Passive Microwave Remote Sensing in a Data-Scarce Environment: A Case Study for Two River Basins in Malawi, Front. Earth Sci., 9, 552, https://doi.org/10.3389/FEART.2021.670997/BIBTEX, 2021.

425 Moriasi, D. N., Gitau, M. W., Pai, N., and Daggupati, P.: Hydrologic and Water Quality Models: Performance Measures and Evaluation Criteria, Trans. ASABE, 58, 1763–1785, https://doi.org/10.13031/TRANS.58.10715, 2015.

Mosavi, A., Ozturk, P., and Chau, K.: Flood Prediction Using Machine Learning Models: Literature Review, Water 2018, Vol. 10, Page 1536, 10, 1536, https://doi.org/10.3390/W10111536, 2018.

Muñoz, D. F., Muñoz, P., Moftakhari, H., and Moradkhani, H.: From local to regional compound flood mapping with deep learning and data fusion techniques, Sci. Total Environ., 782, 146927, https://doi.org/10.1016/J.SCITOTENV.2021.146927, 2021.

Muñoz, D. F., Abbaszadeh, P., Moftakhari, H., and Moradkhani, H.: Accounting for uncertainties in compound flood hazard assessment: The value of data assimilation, Coast. Eng., 171, 104057, https://doi.org/10.1016/J.COASTALENG.2021.104057, 2022.

Naqa, I. El, Ruan, D., Valdes, G., Dekker, A., McNutt, T., Ge, Y., Wu, Q. J., Oh, J. H., Thor, M., Smith, W., Rao, A., Fuller, C., Xiao, Y., Manion, F., Schipper, M., Mayo, C., Moran, J. M., and Haken, R. Ten: Machine learning and modeling: Data, validation, communication challenges, Med. Phys., 45, e834–e840, https://doi.org/10.1002/MP.12811, 2018.

Nayak, P. C., Sudheer, K. P., Rangan, D. M., and Ramasastri, K. S.: Short-term flood forecasting with a neurofuzzy model, Water Resour. Res., 41, 1–16, https://doi.org/10.1029/2004WR003562, 2005.

Planet dump retrieved from https://planet.osm.org: https://www.openstreetmap.org, last access: 20 October 2020.

Pauta, D. F. M.: Tidal influence on the discharge distribution at two junctions of the Kapuas River (West Kalimantan, Indonesia), 2018.

Remacle, J. F. and Lambrechts, J.: Fast and Robust Mesh Generation on the Sphere-Application to Coastal Domains, in: Procedia Engineering, 20–32, https://doi.org/10.1016/j.proeng.2016.11.011, 2016.

Sampurno, J., Vallaeys, V., Ardianto, R., and Hanert, E.: Modeling interactions between tides, storm surges, and river discharges in the Kapuas River delta, Biogeosciences Discuss. [preprint], https//doi.org/10.5194/bg-2021-273, Rev. 2021., https://doi.org/10.5194/BG-2021-273, 2021.

Sanchez, P. A., Ahamed, S., Carré, F., Hartemink, A. E., Hempel, J., Huising, J., Lagacherie, P., McBratney, A. B., McKenzie, N. J., De Lourdes Mendonça-Santos, M., Minasny, B., Montanarella, L., Okoth, P., Palm, C. A., Sachs, J. D., Shepherd, K. D., Vågen, T. G., Vanlauwe, B., Walsh, M. G., Winowiecki, L. A., and Zhang, G. L.: Digital soil map of the world, Science (80-.)., 325, 680–681, 2009.

Santiago-Collazo, F. L., Bilskie, M. V., and Hagen, S. C.: A comprehensive review of compound inundation models in low-gradient coastal watersheds, Environ. Model. Softw., 119, 166–181, https://doi.org/10.1016/J.ENVSOFT.2019.06.002, 2019.

Santiago-Collazo, F. L., Bilskie, M. V., Bacopoulos, P., and Hagen, S. C.: An Examination of Compound Flood Hazard Zones for Past, Present, and Future Low-Gradient Coastal Land-Margins, Front. Clim., 3, 76, https://doi.org/10.3389/FCLIM.2021.684035/BIBTEX, 2021.

Semedi, P.: Palm Oil Wealth and Rumour Panics in West Kalimantan, Forum Dev. Stud., 41, 233–252, https://doi.org/10.1080/08039410.2014.901240, 2014.

Singh, R. K., Soni, A., Kumar, S., Pasupuleti, S., and Govind, V.: Zonation of flood prone areas by an integrated framework
460 of a hydrodynamic model and ANN, 21, 80–97, https://doi.org/10.2166/WS.2020.252, 2021.

Tucci, C. E. M. and Villanueva, A. O. N.: Flood control measures in União da Vitoria and Porto União: structural vs. non-structural measures, 1, 177–182, https://doi.org/10.1016/S1462-0758(00)00012-1, 1999.

Structural and non-structural measures: https://www.undrr.org/terminology/structural-and-non-structural-measures, last access: 12 May 2022.

465 Vallaeys, V., Kärnä, T., Delandmeter, P., Lambrechts, J., Baptista, A. M., Deleersnijder, E., and Hanert, E.: Discontinuous Galerkin modeling of the Columbia River's coupled estuary-plume dynamics, Ocean Model., 124, 111–124, https://doi.org/10.1016/j.ocemod.2018.02.004, 2018.

Vallaeys, V., Lambrechts, J., Delandmeter, P., Pätsch, J., Spitzy, A., Hanert, E., and Deleersnijder, E.: Understanding the circulation in the deep, micro-tidal and strongly stratified Congo River estuary, Ocean Model., 167, 101890,
470 https://doi.org/10.1016/J.OCEMOD.2021.101890, 2021.

Wahl, T., Jain, S., Bender, J., Meyers, S. D., and Luther, M. E.: Increasing risk of compound flooding from storm surge and rainfall for major US cities, Nat. Clim. Chang. 2015 512, 5, 1093–1097, https://doi.org/10.1038/nclimate2736, 2015.

Wahyu, A., Kuntoro, A., and Yamashita, T.: Annual and Seasonal Discharge Responses to Forest/Land Cover Changes and Climate Variations in Kapuas River Basin, Indonesia, J. Int. Dev. Coop., 16, 81–100, https://doi.org/10.15027/29807, 2010.

475 Wang, Q. and Wang, S.: Machine Learning-Based Water Level Prediction in Lake Erie, Water 2020, Vol. 12, Page 2654, 12, 2654, https://doi.org/10.3390/W12102654, 2020.

Xu, Z. X. and Li, J. Y.: Short-term inflow forecasting using an artificial neural network model, Hydrol. Process., 16, 2423–2439, https://doi.org/10.1002/HYP.1013, 2002.

Ye, F., Huang, W., Zhang, Y. J., Moghimi, S., Myers, E., Pe'eri, S., and Yu, H. C.: A cross-scale study for compound flooding
480 processes during Hurricane Florence, Nat. Hazards Earth Syst. Sci., 21, 1703–1719, https://doi.org/10.5194/NHESS-21-1703-2021, 2021.
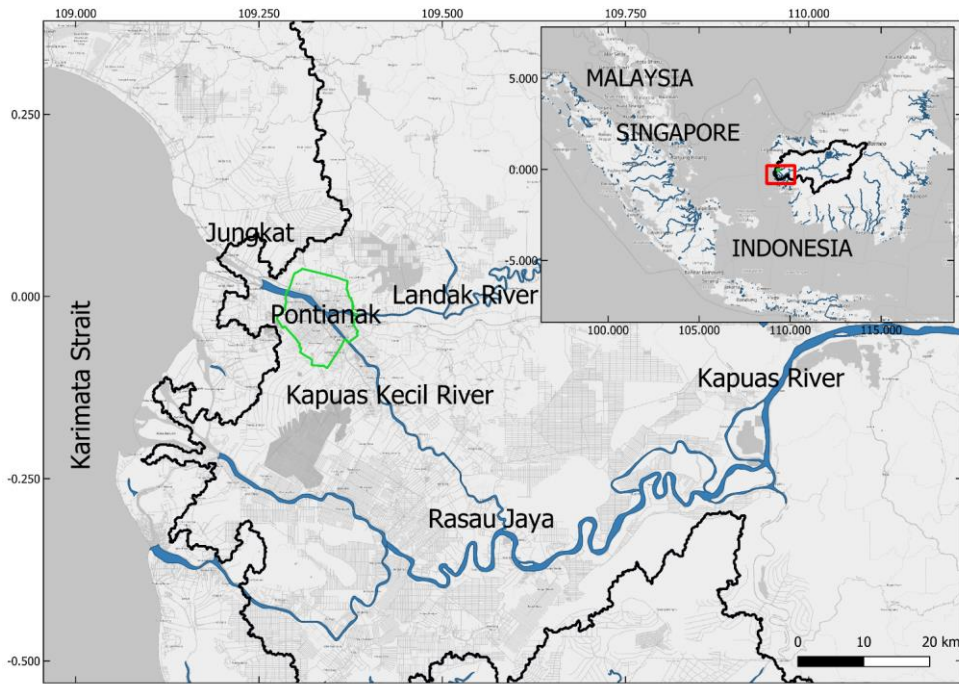
485

Figure 1: The region of interest (ROI), where the green enclosed perimeter represents the city of Pontianak. The solid black line represents the Kapuas River Watershed in the inset map, and the blue lines represent waterbodies. Background map retrieved from (Planet dump retrieved from https://planet.osm.org, 2020). © OpenStreetMap contributors 2017. Distributed under the Open Data Commons Open Database License (ODbL) v1.0.

490

495
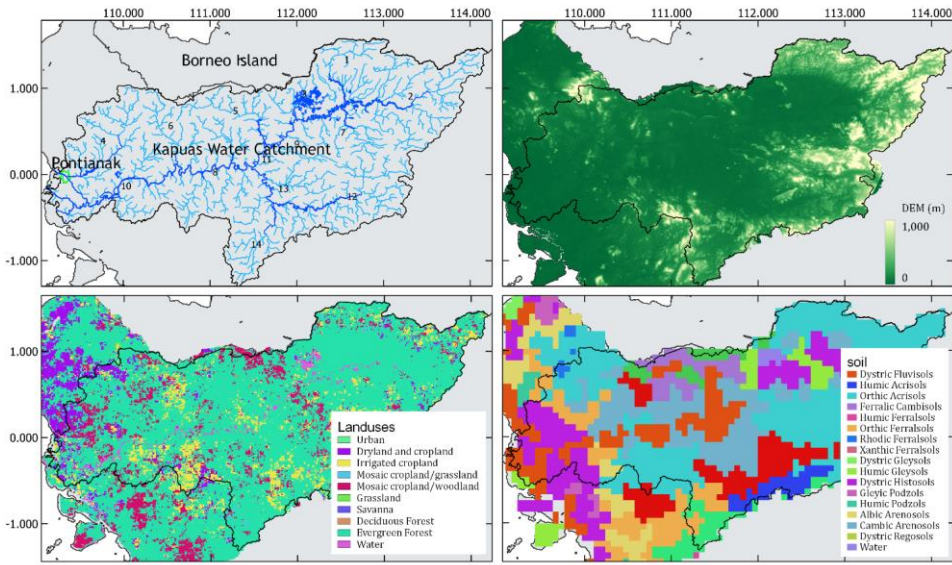
Figure 2: Kapuas water catchment area (upper left), Digital elevation map (upper right) retrieved from SRTM (Farr et al., 2007), Land cover maps (lower left) retrieved from CGLOPS1 (Buchhorn et al., 2020), and Soil type maps (lower right) retrieved from FAO (Sanchez et al., 2009) for the Kapuas River catchment area.
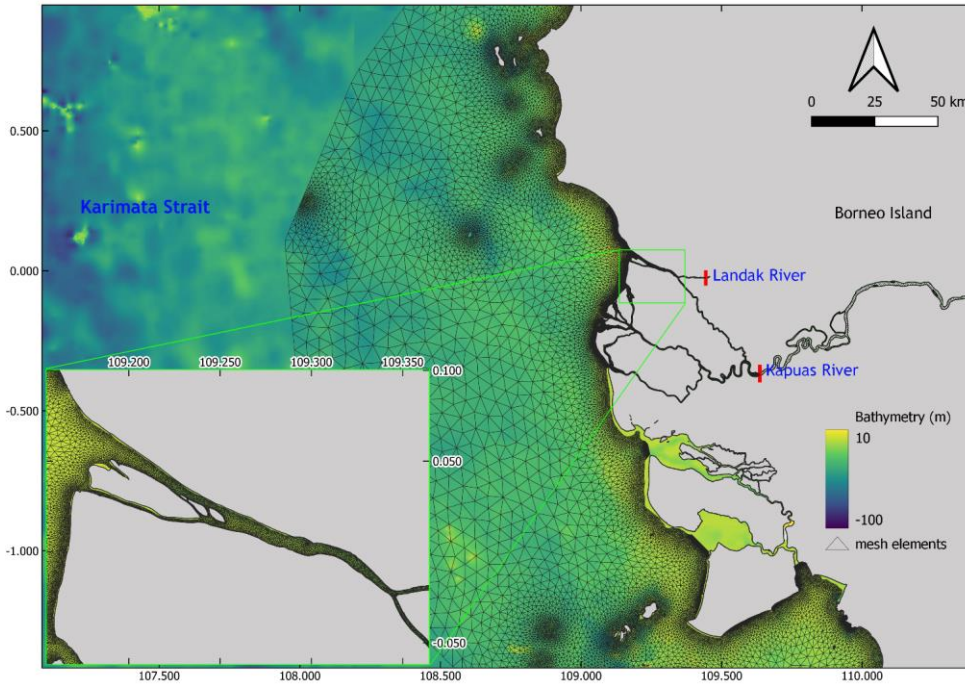
Figure 3: The hydrodynamic model domain is discretized with an unstructured mesh whose resolution is set to 50 m along the riverbanks, 400 m along the coast near the estuary, 1 km over the rest of the coastline, and 5 km offshore. The bathymetry of the model domain ranges from ~100 m depth offshore to 1 m in the river mouth.

505
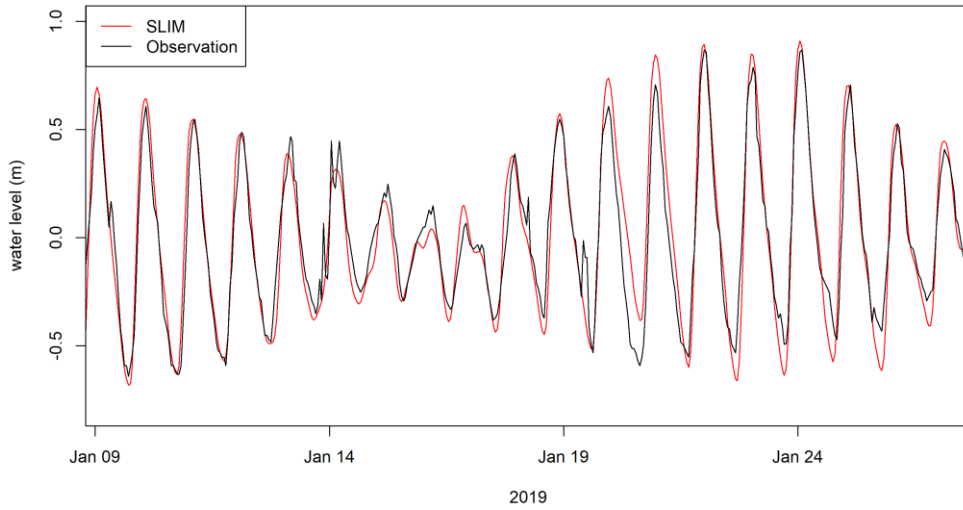
Figure 4: SLIM model output validation with respect to observational data at Pontianak in January 2019, with NSE = 0.87 and RMSE = 0.12 m, indicates that the model has satisfactory performance.

510
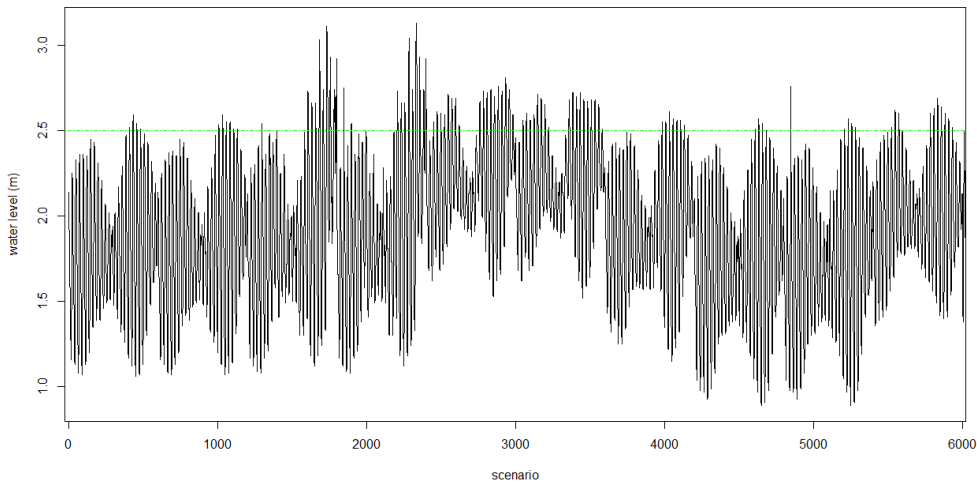
Figure 5: The Kapuas Kecil River's water level in Pontianak, obtained from the hydrodynamic model. The green dash line is the threshold above which the water starts to overflow the riverbanks in Pontianak.
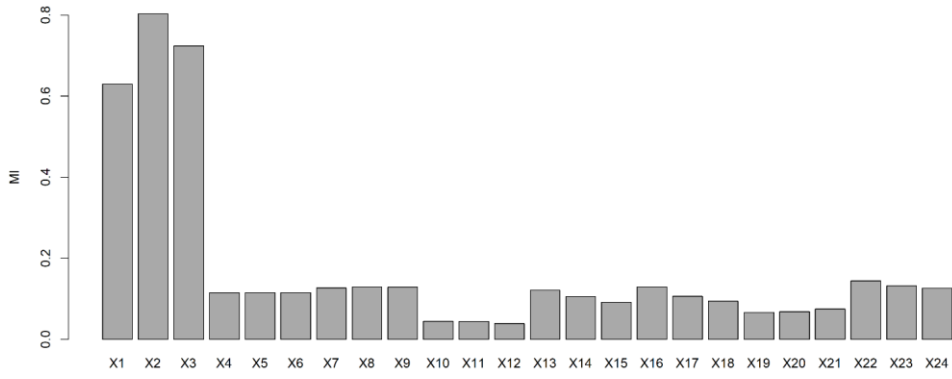
Figure 6: Mutual information of all predictor variables to hourly water level dynamics in 3 months of observational data.

515
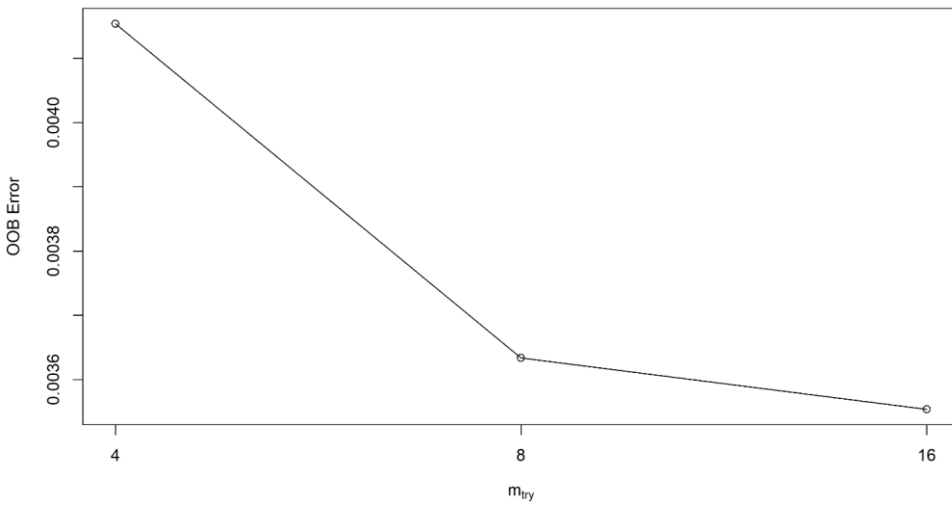
Figure 7: Tuned randomForest algorithm for the optimal number of variables randomly sampled as candidates at each split (mtry) parameter.
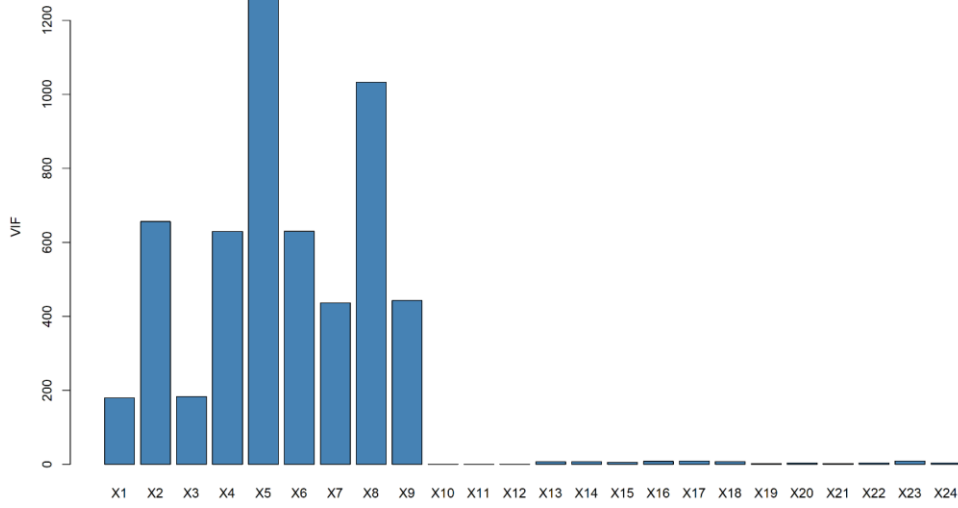
Figure 8: Variance Inflation Factor values of all predictor's variables in 3 months of observational data.
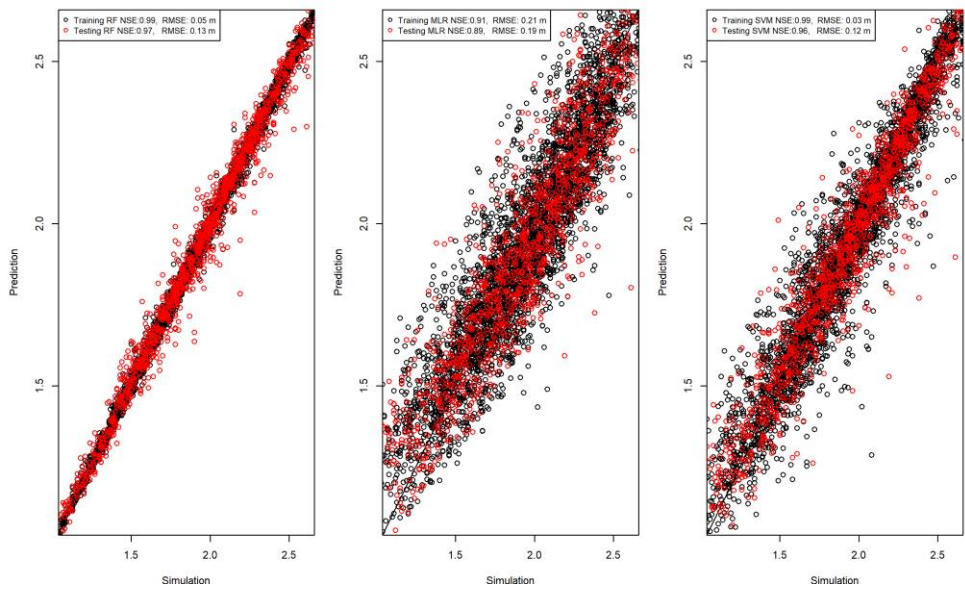
520 **Figure 9:** Comparison of predicted and simulated hourly water levels of the training data.
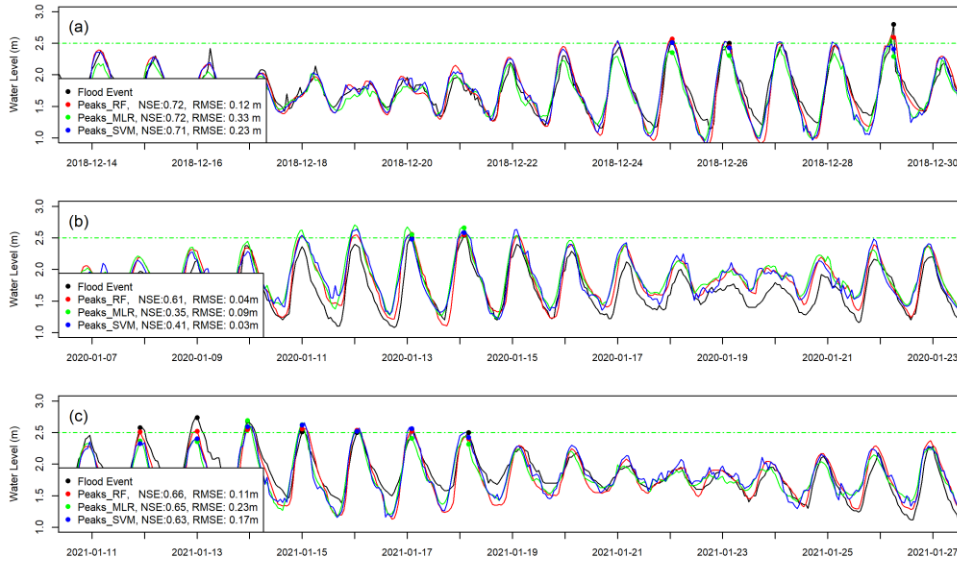
Figure 10: Comparison of predicted hourly water levels models and measured hourly water levels for the implementation phase on: (a)December 2018, (b) January 2020, and (c) January 2021

Table 1. Scenarios used to force the process-based hydrodynamic model

n-dataset	Wind Speed (ms⁻¹)	Wind Direction (°)	Pressure (kPa)	Discharge Kapuas (m³s⁻¹)	Discharge Landak (m³s⁻¹)	Rainfall (mm)
1-600	2 - 8	$0 - 360$	100.5 - 101.5	6×10^3	600	0
601-1200	4-16	$0 - 360$	100.5 - 101.5	6×10^3	600	0
1201-1800	8-32	$0 - 360$	100.5 - 101.5	6×10^3	600	0
1801-2400	$2 - 8$	$0 - 360$	100.5 - 101.5	$10^4 - 1.5 \times 10^4$	600	0
2401-3000	$2 - 8$	$0 - 360$	100.5 - 101.5	6×10^3	800-2100	0
3001-3600	$2 - 8$	$0 - 360$	100.5 - 101.5	$10^4 - 1.5 \times 10^4$	800-2100	0
3601-4200	$5 - 20$	$0 - 360$	100.5 - 101.5	$10^4 - 1.5 \times 10^4$	800-2100	0
4201-4800	$2 - 8$	$0 - 360$	100.5 - 101.5	$3.3 \times 10^3 - 5 \times 10^3$	250-700	0
4801-5400	$2 - 8$	$0 - 360$	100.5 - 101.5	$3.3 \times 10^3 - 5 \times 10^3$	250-700	$0 - 150$
5401-6000	8-32	$0 - 360$	100.5 - 101.5	6×10^3	600	$0 - 150$

Table 2. The variables which used as the predictors in this study.

Code	Variable Description
X1	Tidal Elevation at Kapuas Kecil river mouth (m)
X2	Tidal Elevation at Kapuas Kecil river mouth 1 hour before (m)
X3	Tidal Elevation at Kapuas Kecil river mouth 2 hours before (m)
X4	Hourly Discharge of the Kapuas River at Rasau Jaya in time (m^3s^{-1})
X5	Hourly Discharge of the Kapuas River at Rasau Jaya 1 hour before (m^3s^{-1})
X6	Hourly Discharge of the Kapuas River at Rasau Jaya 2 hours before (m^3s^{-1})
X7	Hourly Discharge of the Landak River at Kuala Mandor in time (m^3s^{-1})
X8	Hourly Discharge of the Landak River at Kuala Mandor 1 hour before (m^3s^{-1})
X9	Hourly Discharge of the Landak River at Kuala Mandor 2 hours before (m^3s^{-1})
X10	Hourly Precipitation at the time (mm)
X11	Hourly Precipitation one hour before (mm)
X12	Hourly Precipitation two hours before (mm)
X13	Hourly Average Wind Speed at the time (ms^{-1})
X14	Hourly Average Wind Speed one hour before (ms^{-1})
X15	Hourly Average Wind Speed two hours before (ms^{-1})
X16	Hourly Maximum Instantaneous Wind Speed at the time (ms^{-1})
X17	Hourly Maximum Instantaneous Wind Speed one hour before (ms^{-1})
X18	Hourly Maximum Instantaneous Wind Speed two hours before (ms^{-1})
X19	Hourly Average Wind Direction at the time (degree, in the range: 0 - 360)
X20	Hourly Average Wind Direction one hours before (degree, in the range: 0 - 360)
X21	Hourly Average Wind Direction two hours before (degree, in the range: 0 - 360)
X22	Hourly Atmospheric Pressure at the time (millibars)
X23	Hourly Atmospheric Pressure one hour before (millibars)
X24	Hourly Atmospheric Pressure two hours before (millibars)

Table 3. Performance of the three machine learning algorithms on implementation phase

Goodness of Fit	RF	MLR	SVM
NSE Training	0.99	0.91	0.99
NSE Testing	0.97	0.96	0.89
NSE Implementation1 (Dec 2018)	0.72	0.72	0.71
NSE Implementation2 (Jan 2020)	0.61	0.35	0.41
NSE Implementation3 (Jan 2021)	0.66	0.65	0.63
Total of flood predicted (out of 17 events)	11	6	10
Percent of flood predicted	65%	35%	59%
False Positive (event)	4	3	3